Hydrol. Earth Syst. Sci. Discuss., 12, 6467–6503, 2015
www.hydrol-earth-syst-sci-discuss.net/12/6467/2015/
doi:10.5194/hessd-12-6467-2015

Hydrology and Earth System Sciences
Open Access
Discussions

Estimating spatially distributed soil water content at small watershed scales based on decomposition of temporal anomaly and time stability analysis

W. Hu and B. C. Si

University of Saskatchewan, Department of Soil Science, Saskatoon, SK S7N 5A8, Canada

Received: 20 April 2015 – Accepted: 04 June 2015 – Published: 03 July 2015

Correspondence to: W. Hu (wei.hu@usask.ca)

Published by Copernicus Publications on behalf of the European Geosciences Union.

Abstract

Soil water content (SWC) at watershed scales is crucial to rainfall–runoff response. A model was used to decompose spatiotemporal SWC into time-stable pattern (i.e., temporal mean), space-invariant temporal anomaly, and space-variant temporal anomaly. This model was compared with a previous model that decomposes spatiotemporal SWC into spatial mean and spatial anomaly. The space-variant temporal anomaly or spatial anomaly was further decomposed using the empirical orthogonal function for estimating spatially distributed SWC. These two models are termed temporal anomaly (TA) model and spatial anomaly (SA) model, respectively. We aimed to test the hypothesis that underlying (i.e., time-invariant) spatial patterns exist in the space-variant temporal anomaly at the small watershed scale, and to examine the advantages of the TA model over the SA model in terms of estimation of spatially distributed SWC. For this purpose, a SWC dataset of near surface (0–0.2 m) and root zone (0–1.0 m) from a small watershed scale in the Canadian prairies was analyzed. Results showed that underlying spatial patterns exist in the space-variant temporal anomaly because of the permanent controls of "static" factors such as depth to the $CaCO_3$ layer and organic carbon content. Combined with time stability analysis, the TA model improved estimation of spatially distributed SWC over the SA model because the latter failed to capture the space-variant temporal anomaly which accounted for non-negligible amounts of spatial variance in SWC. The outperformance was greater when SWC deviated from intermediate conditions, especially for dry conditions. Therefore, the TA model has potential to construct a spatially distributed SWC at watershed scales from remote sensed SWC.

1 Introduction

Soil water content (SWC) of surface soils exerts a major influence on a series of hydrological processes such as runoff and infiltration (Famiglietti et al., 1998;

HESSD
12, 6467–6503, 2015

Vereecken et al., 2007; She et al., 2013a). Soil water content of the root zone is usually linked to vegetative growth (Wang et al., 2012; Ward et al., 2012; Jia and Shao, 2013). Accurate information on spatiotemporal SWC is a prerequisite for improving hydrological prediction and soil water management (Venkatesh et al., 2011; Champagne et al., 2012; She et al., 2013b; Zhao et al., 2013). While remote sensing has advanced SWC measurements of surface soils (< 5 cm thick) at basin (2500–25 000 km^2) and continental scales (Robinson et al., 2008), characterization of spatially distributed SWC at small watershed (0.1–80 km^2) scales still poses a challenge. A method is needed for estimating spatially distributed SWC in the near surface and root zone at watershed scales.

Time stability of SWC, referring to similar spatial patterns of SWC across different measurement times (Vachaud et al., 1985; Brocca et al., 2009), has been used for estimating spatially distributed SWC (Starr, 2005; Perry and Niemann, 2007; Blöschl et al., 2009). This method is conceptually-appealing, but assumes completely time-stable spatial patterns of SWC.

The time-stable pattern does not explain all of the spatial variances in SWC, indicating the existence of time-variant components (Starr, 2005). In order to identify underling patterns of SWC that have time-variant components, spatiotemporal SWC was decomposed into spatial mean and spatial anomaly, with the latter being further decomposed into the sum of the product of time-invariant spatial patterns (EOFs) and temporally varying but spatially constant coefficients (ECs) by the empirical orthogonal function (EOF) (Fig. 1) (Jawson and Niemann, 2007; Perry and Niemann, 2007, 2008; Joshi and Mohanty, 2010; Korres et al., 2010; Busch et al., 2012). Spatially distributed SWC estimates based on the decomposition of spatial anomaly outperformed those based on time-stable patterns (Perry and Niemann, 2007).

Recently, spatiotemporal SWC was also decomposed into temporal mean and temporal anomaly (Mittelbach and Seneviratne, 2012) (Fig. 1). Previous studies indicated that the contribution of temporal anomaly to the total spatial variance was notable (Mittelbach and Seneviratne, 2012; Brocca et al., 2014; Rötzer et al., 2015).

HESSD
12, 6467–6503, 2015

These studies, however, only focused on surface soils and large scales ($>250\,km^2$). Vanderlinden et al. (2012) suggested that the temporal mean be further decomposed into its spatial mean and residuals, and the temporal anomaly be further decomposed into space-invariant term (i.e., spatial mean of temporal anomaly) and space-variant term (i.e., spatial residuals of temporal anomaly) (Fig. 1). Note that the spatial variance in the temporal anomaly (Mittelbach and Seneviratne, 2012) equals that in the space-variant term of temporal anomaly (Vanderlinden et al., 2012). The further decomposition of temporal anomaly may be physically meaningful, because the space-invariant and space-variant terms in the temporal anomaly may be forced differently. However, the models of Mittelbach and Seneviratne (2012) and Vanderlinden et al. (2012) have not been used for estimating spatially distributed SWC. If the space-variant terms are ignored during the estimation of spatially distributed SWC, their models are equivalent to that based on time-stable patterns. Therefore, estimation of spatially distributed SWC may be improved by incorporating the space-variant term of temporal anomaly if underlying (i.e., time-invariant) spatial patterns exist in it.

To our knowledge, the importance of space-variant term of temporal anomaly and its physical meaning at small watershed scales is not well-known. Based on previous studies (Perry and Niemann, 2007; Mittelbach and Seneviratne, 2012; Vanderlinden et al., 2012), we assume soil water dynamics at watershed scales can be decomposed into three components (Fig. 1): (1) time-stable pattern (i.e., temporal mean, spatial forcing): the "static" factors such as soil and topography control the pattern; (2) space-invariant temporal anomaly (temporal forcing): the "dynamic" factors such as meteorological variables and vegetation change with time, and therefore modify SWC in time, regardless of spatial locations; and (3) space-variant temporal anomaly (interactions between spatial forcing and temporal forcing): this term represents interactions between "static" and "dynamic" factors. For example, SWC recharge introduced by a rainfall may be modified by topography through runoff processes; SWC loss triggered by evapotranspiration may be regulated by topography through solar radiation exposure.

HESSD
12, 6467–6503, 2015

The "static" factors can be persistent in the space-variant temporal anomaly, and their impacts on the space-variant temporal anomaly likely change with time. Thus, we hypothesize that some underlying (i.e., time-invariant) spatial patterns exist in the space-variant temporal anomaly, and their impacts can be modulated by a time coefficient, both of which can be obtained by the EOF method (Fig. 1). If the hypothesis is true, estimation of spatially distributed SWC utilizing the EOF decomposition may outperform the one suggested by Perry and Niemann (2007). This is because: (1) the spatial anomaly which was decomposed using the EOF in Perry and Niemann (2007) lumped the time-stable pattern and space-variant temporal anomaly together (Fig. 1); (2) the underlying spatial patterns in the spatial anomaly may not fully capture both time-stable patterns and patterns in the space-variant temporal anomaly due to the possible nonlinear relations between these two terms.

Therefore, the objectives were (1) to test the hypothesis that underlying spatial patterns exist in the space-variant temporal anomaly at small watershed scales and (2) to examine whether the decomposition of space-variant temporal anomaly using the EOF has any advantages over the decomposition of spatial anomaly (Perry and Niemann, 2007) for estimating spatially distributed SWC. Two steps were included in the estimation of spatially distributed SWC. First, spatial mean SWC was upscaled from SWC measurement at the most time-stable location using the time stability analysis. Then spatially distributed SWC was downscaled from the estimated spatial mean SWC. For this purpose, spatiotemporal SWC datasets from depths of near surface (0–0.2 m) and root zone (0–1.0 m) from a Canadian prairie landscape were used.

2 Materials and methods

2.1 Study area and data collection

The study area is located in St. Denis National Wildlife Area (52°12′ N, 106°50′ W) and has an area of 3.6 km^2 in the Canadian prairies. This area has a humid continental

HESSD
12, 6467–6503, 2015

climate (Peel et al., 2007). A variety of depressions, knolls, and knobs result in a sequence of undulating slopes (Biswas et al., 2011). The soils are dominated by Mollisols (Soil Survey Staff, 2010). Near surface soil porosity ranges from 38 % (knolls) to 70 % (depressions). A sampling transect 576 m long with 128 sampling locations spaced at 4.5 m intervals was established over several rounded knolls and depressions. At each location, a time domain reflectometry probe was used to measure SWC of the near surface soil (0–0.2 m), and a neutron probe was used to collect SWC measurements at 0.2 m intervals between a depth of 0.2 and 1.0 m. The SWC of the root zone was calculated by averaging the SWC of 0–0.2, 0.2–0.4, 0.4–0.6, 0.6–0.8, and 0.8–1.0 m. Soil water content was measured on 23 dates from 17 July 2007 to 29 September 2011. The SWC dataset, collected in all seasons except winter, accurately portrays the variations in soil water conditions in the study area. In addition to the SWC dataset, the soil, vegetative, and topographical properties were obtained at each sampling location (Biswas et al., 2012). These properties were used to relate time-stable patterns and underlying spatial patterns of space-variant temporal anomaly to environmental factors.

2.2 Statistical models for decomposing soil water content

Spatiotemporal SWC at small watershed scales was decomposed into three components: time-stable pattern, space-invariant temporal anomaly, and space-variant temporal anomaly. For estimation of spatially distributed SWC, further decomposition of space-variant temporal anomaly was conducted using the EOF method. In order to show advantages of this model over the one developed by Perry and Niemann (2007), SWC was also decomposed into spatial mean and spatial anomaly, with the latter being further decomposed using the EOF method. The two models are termed temporal anomaly (TA) model and spatial anomaly (SA) model, respectively. Please refer to Fig. 1 for the differences of the two models. Each component will be explained in detail later. Because we focus on estimating spatial distribution of SWC at any given

HESSD
12, 6467–6503, 2015

time, only spatial variances of SWC were taken into account in this study. Therefore, the variance or covariance denotes the quantity in space without specifications.

2.2.1 The SA model

Perry and Niemann (2007) expressed SWC at location n and time t, S_{tn}, as (Fig. 1):

$$S_{tn} = S_{t\hat{n}} + Z_{tn}, \quad (1)$$

where $S_{t\hat{n}}$ is the spatial mean SWC at time t (temporal forcing) and Z_{tn} is the spatial anomaly of SWC (lumped spatial forcing and interactions). The subscript $\hat{n}$ ($\hat{t}$) indicates a space (time) averaged quantity.

$S_{t\hat{n}}$ in Eq. (1) was obtained from SWC at the most time-stable location s and time t, S_{ts}, using (Grayson and Western, 1998):

$$S_{t\hat{n}} = \frac{S_{ts}}{1 + \delta_{\hat{t}s}}, \quad (2)$$

where the most time-stable location s was identified using time stability index of mean absolute bias error (Hu et al., 2010, 2012). $\delta_{\hat{t}s}$ is the temporal mean relative difference of SWC at the most time-stable location s calculated with prior measurements.

Spatial anomaly Z_{tn} is decomposed into a series of time-invariant spatial patterns (EOFs) (Perry and Niemann, 2007). The sum of products of the EOFs and the temporally varying (but spatially constant) coefficients (ECs) leads to the reconstructed original Z_{tn} in a space-time domain (Joshi and Mohanty, 2010; Vanderlinden et al., 2012). The number of EOF (or EC) series equals the number of sampling dates. Each EOF series corresponds to one value at each location, and each EC series has one value at each measurement time. The ith EOF is chosen to be orthogonal to the first through $(i - 1)$th EOF, and accounts for as much variance as possible. The sum of variances of all EOFs equals the sum of variances of Z_{tn} from all measurement times.

Usually, a substantial amount of variance can be explained by a small number of EOFs. Johnson and Wichern (2002) suggested the eigenvalue confidence limits

HESSD
12, 6467–6503, 2015

method for selecting the number of EOFs. Once the number of significant EOFs at a confidence level of 95 % is selected, Z_{tn} can be estimated as the sum of the product of significant EOFs and associated ECs as:

$$Z_{tn} = \sum \mathrm{EOF}^{\mathrm{sig}} \cdot \left(\mathrm{EC}^{\mathrm{sig}}\right)^{T}, \tag{3}$$

where $\mathrm{EOF}^{\mathrm{sig}}$ represents the significant EOFs of the Z_{tn} obtained during model development, $\mathrm{EC}^{\mathrm{sig}}$ is the associated temporally varying coefficient and superscript T represents matrix transpose. The associated significant EC at time t, EC_t, can be estimated by the cosine relationship between EC and $S_{t\hat{n}}$ developed using prior measurements (Perry and Niemann, 2007):

$$\mathrm{EC}_t = a + b\cos\left(\frac{2\pi}{c}S_{t\hat{n}} - d\right), \tag{4}$$

where a, b, c, and d are fitted parameters using prior measurements and $S_{t\hat{n}}$ is estimated from Eq. (2).

2.2.2 The TA model

Mittelbach and Seneviratne (2012) decomposed the variance of S_{tn} into a time-stable pattern (i.e., temporal mean) and a temporal anomaly component (Fig. 1):

$$S_{tn} = M_{\hat{t}n} + A_{tn}, \tag{5}$$

where $M_{\hat{t}n}$ is the time-stable pattern (spatial forcing), which is controlled by temporally-constant but spatially-varying factors such as soil properties and topography; and A_{tn} refers to the temporal anomaly (lumped temporal forcing and interactions). The variance of SWC, $\sigma^2_{\hat{n}}(S_{tn})$, is the sum of variance of the $M_{\hat{t}n}$, $\sigma^2_{\hat{n}}(M_{\hat{t}n})$, the variance of the A_{tn}, $\sigma^2_{\hat{n}}(A_{tn})$, and two times of covariance between $M_{\hat{t}n}$ and A_{tn}, $2\mathrm{cov}(M_{\hat{t}n}, A_{tn})$,

HESSD
12, 6467–6503, 2015

which can be expressed as:

$$\sigma^2_{\hat{n}}(S_{tn}) = \sigma^2_{\hat{n}}(M_{\hat{t}n}) + 2\mathrm{cov}(M_{\hat{t}n}, A_{tn}) + \sigma^2_{\hat{n}}(A_{tn}). \quad (6)$$

Because A_{tn} in Mittelbach and Seneviratne (2012) is a lumped term, it can be further decomposed into space-invariant temporal anomaly $A_{t\hat{n}}$ (temporal forcing) and space-variant temporal anomaly R_{tn} (interactions) as Vanderlinden et al. (2012) suggested. At a watershed scale, $A_{t\hat{n}}$ is controlled by spatially-constant but temporally varying factors such as meteorological variables and vegetation (vegetation usually has greater variations over time than over space at small watershed scales). Positive and negative $A_{t\hat{n}}$ correspond to relatively wet and dry periods, respectively. The R_{tn} refers to the redistribution of $A_{t\hat{n}}$ among different locations due to the interactions between spatial forcing and temporal forcing. For example, soil and topography regulate how much rainfall enters soil and how much water runs off or runs on at a location, resulting in spatial variability in temporal anomaly. This, in turn, dictates vegetation growth in a water-limited environment. Therefore, S_{tn} can be expressed as (Fig. 1):

$$S_{tn} = M_{\hat{t}n} + A_{t\hat{n}} + R_{tn}. \quad (7)$$

The temporal trends of $A_{t\hat{n}}$ in Eq. (7) and $S_{t\hat{n}}$ in Eq. (1) are the same, as both represent temporal forcing. Because $A_{t\hat{n}}$ is space-invariant and orthogonal to $M_{\hat{t}n}$ and R_{tn} in a space, $\sigma^2_{\hat{n}}(S_{tn})$ in Eq. (6) can also be written as:

$$\sigma^2_{\hat{n}}(S_{tn}) = \sigma^2_{\hat{n}}(M_{\hat{t}n}) + 2\mathrm{cov}(M_{\hat{t}n}, R_{tn}) + \sigma^2_{\hat{n}}(R_{tn}), \quad (8)$$

where $\mathrm{cov}(M_{\hat{t}n}, R_{tn})$ is the covariance between $M_{\hat{t}n}$ and R_{tn}, and $\sigma^2_{\hat{n}}(R_{tn})$ is the variance of the R_{tn}. Apparently, $2\mathrm{cov}(M_{\hat{t}n}, R_{tn})$ equals $2\mathrm{cov}(M_{\hat{t}n}, A_{tn})$, and $\sigma^2_{\hat{n}}(R_{tn})$ equals $\sigma^2_{\hat{n}}(A_{tn})$. If R_{tn} is zero at any time or location, there are no interactions between spatial forcing and temporal forcing, $\sigma^2_{\hat{n}}(S_{tn})$ and the spatial trends of SWC are consistent over time. Therefore, R_{tn} is directly responsible for a temporal change in spatial variability of SWC.

HESSD
12, 6467–6503, 2015

If some underlying spatial patterns exist in R_{tn}, R_{tn} can be reconstructed by the sum of the product of time-invariant spatial structures (EOFs) and time-dependent coefficients (ECs) using the EOF method. Note that the number of EOF (or EC) series also equals the number of sampling dates.

For estimation of spatially distributed SWC, R_{tn} is estimated by the same method as Z_{tn} using Eq. (3). The $M_{\hat{t}n}$ is estimated with prior measurements by:

$$M_{\hat{t}n} = \frac{1}{m}\sum_{j=1}^{m} S_{tn}, \tag{9}$$

where m is the number of previous measurement times, and $A_{t\hat{n}}$ is estimated by:

$$A_{t\hat{n}} = S_{t\hat{n}} - M_{\hat{t}\hat{n}}, \tag{10}$$

where $M_{\hat{t}\hat{n}}$ is the spatial mean of $M_{\hat{t}n}$, and $S_{t\hat{n}}$ is estimated from SWC measurements at the most time-stable location using Eq. (2).

2.3 Validation and performance parameter

The TA model is more complicated than the SA model. In order to evaluate the two models for parsimony, AICc values are calculated (Burnham and Anderson, 2002) as:

$$\mathrm{AICc} = 2k + n\ln(\mathrm{RSS}/n) + 2k(k+1)/(n-k-1), \tag{11}$$

where k is the number of parameters, n is the sample size, and RSS is the residual sum of squares.

Cross validation is used to estimate SWC distribution along the transect with both models. An iterative removal of 1 of the 23 dates is made for model development, and the SWC along the transect corresponding to the removed date is estimated iteratively.

HESSD
12, 6467–6503, 2015

The Nash–Sutcliffe coefficient of efficiency (NSCE) is used to evaluate the quality of estimation of spatially distributed SWC, which is expressed as:

$$\mathrm{NSCE} = 1 - \frac{\sigma_{\varepsilon}^2}{\sigma_{\mathrm{measure}}^2}, \tag{12}$$

where $\sigma_{\mathrm{measure}}^2$ is the variance of measured SWC, and σ_{ε}^2 is the mean squared estimation error. A larger NSCE value implies a better quality of estimation.

3 Results

3.1 Components of SWC and their controls

3.1.1 Spatial mean $S_{t\hat{n}}$ and spatial anomaly Z_{tn}

The values of spatial mean $S_{t\hat{n}}$ in the SA model varied with seasons (Fig. 2a). In the spring, such as 02 May 2008 and 20 April 2009, snowmelt infiltration resulted in relatively great $S_{t\hat{n}}$ values. In the summer, however, even one month after large rainfall events (such as on 19 July 2008 and 21 June 2009), the high evapotranspiration by fast-growing vegetation resulted in small $S_{t\hat{n}}$. The values of $S_{t\hat{n}}$ also varied between inter-annual meteorological conditions. In 2008, there was less precipitation and higher air temperature than in 2010. As a result, $S_{t\hat{n}}$ was relatively smaller in 2008 than in 2010.

The spatial patterns of spatial anomaly Z_{tn} on two individual dates that had contrasting soil water conditions are shown in Fig. 2b. The values of Z_{tn} in a wet period (13 May 2011) were much greater than in a dry period (23 August 2008) in depressions (e.g., at a distance of 123 and 250 m); at other locations, however, the spatial anomaly was slightly less in a wet period than in a dry period for both soil layers. Moreover, the spatial anomaly in depressions during wet periods was much greater in the near surface than in the root zone.

HESSD
12, 6467–6503, 2015

When SWCs of all 23 dates were used for model development, only EOF1 was statistically significant (Fig. 3a), which accounted for 84.3 % (0–0.2 m) and 86.5 % (0–1.0 m) of the variances in the Z_{tn}. Correlation analysis indicated that the spatial pattern of EOF1 in the Z_{tn} was identical to the time-stable patterns $M_{\hat{t}n}$ in the TA model ($R = 1.0$). The controls of EOF1 was therefore the same as those of $M_{\hat{t}n}$, and will be discussed later. The relation between associated EC1 and $S_{t\hat{n}}$ can be fitted well by the cosine function (Fig. 3b).

3.1.2 Time-stable pattern $M_{\hat{t}n}$, space-invariant temporal anomaly $A_{t\hat{n}}$, and space-variant temporal anomaly R_{tn}

Figure 4 displays the three components in the TA model. The first component $M_{\hat{t}n}$ fluctuated along the transect, with high values in depressions and low values on knolls (Fig. 4a); $M_{\hat{t}n}$ also had greater spatial variability in the near surface (variance = 36.7 %^{2}) than in the root zone (variance = 19.5 %^{2}). For both soil layers, soil organic carbon content (SOC), depth to the $CaCO_3$ layer, sand content, and wetness index are the dominant factors of $M_{\hat{t}n}$; they together explained 74.5 % (near surface) and 75.6 % (root zone) of the variances in $M_{\hat{t}n}$ (Table 1). In addition, the temporal trend of $A_{t\hat{n}}$ (Fig. 4b) was the same as that of $S_{t\hat{n}}$ in the SA model (Fig. 2b), as both represent temporal forcing.

The R_{tn} varied among landscape positions (Fig. 4c). At a sampling distance of 123 m (in a depression), R_{tn} was negative in dry periods such as 23 August 2008 and positive in wet periods such as 13 May 2011. This was true for all depressions for both the near surface and the root zone. Therefore, topographically lower positions usually corresponded to more positive R_{tn} during the wet period and more negative R_{tn} during the dry period. This implies that topographically lower locations gained more water during recharge and lost more water during discharge due to the interactions of spatial and temporal forcing. Furthermore, the absolute values of R_{tn} were generally greater in the near surface than the root zone, indicating greater space-variant temporal anomaly for shallower depths.

HESSD
12, 6467–6503, 2015

The SWC variances and associated components (Eq. 8) also varied with time (Fig. 5). Often, wetter conditions corresponded to greater $\sigma^2_{\hat{n}}(S_{tn})$, as further indicated by moderate correlation between $\sigma^2_{\hat{n}}(S_{tn})$ and $S_{t\hat{n}}$ (R^2 of 0.51 and 0.38 for the near surface and the root zone, respectively). This was in agreement with others (Gómez-Plaza et al., 2001; Martínez-Fernández and Ceballos, 2003; Hu et al., 2011). Furthermore, there were greater $\sigma^2_{\hat{n}}(S_{tn})$ values at near surface than root zone, indicating greater variability of SWC in the near surface.

The time-invariant $\sigma^2_{\hat{n}}(M_{\hat{t}n})$ contributed to the $\sigma^2_{\hat{n}}(S_{tn})$ with percentages ranging from 25 to 795 % for the near surface and from 40 to 174 % for the root zone (Fig. 5). The $\sigma^2_{\hat{n}}(M_{\hat{t}n})$ exceeded $\sigma^2_{\hat{n}}(S_{tn})$ mainly under dry conditions, such as July–October in 2008 and 2009. This excess was offset by $\sigma^2_{\hat{n}}(S_{tn})$ and $2\mathrm{cov}(M_{\hat{t}n}, R_{tn})$, and the latter contributed negatively to $\sigma^2_{\hat{n}}(S_{tn})$ with mean percentages of 210 % for the near surface and 17 % for the root zone. In the dry period, the negative contribution from $2\mathrm{cov}(M_{\hat{t}n}, R_{tn})$ was up to 1327 % for the near surface and 122 % for the root zone. These values are comparable to those in Mittelbach and Seneviratne (2012) and Brocca et al. (2014).

The $\sigma^2_{\hat{n}}(R_{tn})$ contributed less than other components (Fig. 5). The percentages of $\sigma^2_{\hat{n}}(R_{tn})$ ranged from 11 to 632 % (average of 118 %) for the near surface and from 6 to 48 % (average of 19 %) for the root zone; $\sigma^2_{\hat{n}}(R_{tn})$ tended to contribute more in drier periods. This indicates that space-variant temporal anomaly cannot be ignored, particularly in dry conditions. Furthermore, the contribution of $\sigma^2_{\hat{n}}(R_{tn})$ was greater in the near surface than in the root zone, confirming stronger temporal dynamics of soil water at the near surface. Compared with larger scale studies (Mittelbach and Seneviratne, 2012; Brocca et al., 2014), $\sigma^2_{\hat{n}}(R_{tn})$ of the near surface in this study contributed more to $\sigma^2_{\hat{n}}(S_{tn})$, with a mean percentage contribution of 118 %, versus 9–68 % in other studies (Mittelbach and Seneviratne, 2012; Brocca et al., 2014). This indicates that interactions between spatial and temporal forcing were stronger, resulting

HESSD
12, 6467–6503, 2015

in relatively more intensive temporal dynamics of soil water in our study area than at larger scales.

Three significant EOFs of R_{tn} for both soil layers were identified when SWC of all 23 dates were used for model development. The first three EOFs explained 61.1, 13.4, and 8.1 % respectively, of the total R_{tn} variance for the near surface, and 44.3, 20.2, and 12.4, respectively, of the total R_{tn} variance for the root zone. Therefore, our hypothesis that underlying spatial patterns exist in the R_{tn} was accepted. Due to the negligible contribution of EOF2 and EOF3 to the estimation of spatially distributed SWC, only EOF1 is shown in Fig. 6a. The associated EC1 changed with soil water conditions ($S_{t\hat{n}}$) (Fig. 6b). When SWC was close to average levels, the EC1 was close to 0, resulting in negligible R_{tn}. This was in accordance with Mittelbach and Seneviratne (2012) and Brocca et al. (2014), who showed that the spatial variance of temporal anomaly was the smallest when water contents were close to average levels. The cosine function (Eq. 11) explained a large amount of the variances in EC1 for both soil layers ($R^2 = 0.76$ at the near surface and 0.88 in the root zone).

The contribution of EOF1 to the space-variant temporal anomaly can be examined through the product of the EOF1 and the associated EC1. EC1 values tended to be positive during wet periods and negative during dry periods (Fig. 6b); more positive EOF1 values were usually observed at locations with greater $M_{\hat{t}n}$ values (Figs. 4a and 6a). Therefore, the product of EOF1 and EC1 led to greater temporal SWC dynamics at wetter locations of both layers in both the wet and dry periods.

Depth to the $CaCO_3$ layer and SOC had significant, positive correlations with EOF1 for both soil layers (R ranging from 0.76 to 0.88; Table 1). They jointly accounted for 81.6 % (near surface) and 81.0 % (root zone) of the variances in EOF1. This implies that locations with a greater depth to the $CaCO_3$ layer and SOC, which correspond to wetter locations such as depressions, usually have greater temporal SWC dynamics during both wet and dry periods.

HESSD
12, 6467–6503, 2015

3.2 Estimation of spatially distributed SWC

When all 23 datasets were used and only EOF1 was considered, the TA model had an AICc value of 4093 for the near surface and 562 for the root zone, while the corresponding values for the SA model were 6370 and 3460. This indicated that even when penalty to complexity was given, the TA model was better than the SA model. The two models in terms of estimation of spatially distributed SWC are compared below.

3.2.1 The TA model

The R_{tn} terms and associated EOFs differed slightly with each validation. The number of significant EOFs varied between one (accounting for 60 % of the total cases) and three for both soil layers. A Paired Samples T-test indicated that more EOFs did not result in a significant increase of NSCE in the estimation of spatially distributed SWC, because AICc values increased greatly with the increasing number of parameters resulting from more EOFs (data not shown). This indicates that higher-order EOFs, even if they are statistically significant, are negligible for SWC prediction. Therefore, SWC distribution was estimated with EOF1 only.

Estimated SWCs generally approximated those measured at different soil water conditions (Fig. 7). However, on 27 October 2009, there were unsatisfactory estimates at the 100–140 and 220–225 m locations near the surface. Unsatisfactory NSCE values of 4.05, −1.83, and −3.81 were obtained in the near surface in only three of the 23 dates, which were all in the fall (22 October 2008, 27 August 2009, and 27 October 2009, respectively). The poor performance obtained with the TA model on those dates was a result of overestimation in depressions, where strong evapotranspiration and deep drainage resulted in much lower SWC than in the spring. These dates also corresponded to a high percentage of contribution of $\sigma^2_{\hat{n}}(R_{tn})$ to $\sigma^2_{\hat{n}}(S_{tn})$ (203–439 %). For 23 August and 17 September in 2008, which were in dry periods, $\sigma^2_{\hat{n}}(R_{tn})$ of the near surface also contributed highly to $\sigma^2_{\hat{n}}(S_{tn})$ (580 and 630 %). Because a fair amount

HESSD
12, 6467–6503, 2015

of $\sigma^2_{\hat{n}}(R_{tn})$ was accounted for with the TA model, the TA model performed satisfactorily (NSCE of 0.43 and 0.60).

For the remaining 20 dates, the resulting NSCE value ranged from 0.38 to 0.90 in the near surface and from 0.65 to 0.96 in the root zone (Fig. 8). This suggests that the TA model was generally satisfactory, with better performance in the root zone than in the near surface.

3.2.2 Comparison with the SA model

One significant EOF of Z_{tn} was identified in each validation for both soil layers. The SA model with only EOF1 produced reasonable SWC estimations in all dates in the root zone and in every date except five dates (23 August 2008, 17 September 2008, 22 October 2008, 27 August 2009, and 27 October 2009) in the near surface (Fig. 8). Similarly, when more EOFs were included, NSCE values did not increase significantly (data not shown) and consequently, estimation of spatially distributed SWC was not improved. This was because EOF2 and EOF3 together explained a very limited ($< 10\,\%$) amount of variability of Z_{tn} and thus had low predictive power in terms of variance.

The difference in NSCE values between the TA and SA models are presented in Fig. 9. Generally, the difference decreased as $A_{t\hat{n}}$ increased, and then slightly increased with a further increase in $A_{t\hat{n}}$. The TA model outperformed the SA model, as indicated by a positive NSCE difference, particularly in dry conditions. This was because when soil was dry, there was a high contribution of $\sigma^2_{\hat{n}}(R_{tn})$, and thus strong variability in the space-variant temporal anomaly.

4 Discussion

Space-variant temporal anomaly R_{tn} played an important role in the temporal change of spatial patterns in SWC. The underlying spatial patterns and physical meaning

HESSD
12, 6467–6503, 2015

in the R_{tn} were examined in our study for the first time. Although three significant EOFs existed in the R_{tn} for some cases, only EOF1 was needed for the estimation of spatially distributed SWC with the TA model. Among many factors influencing the EOF1 of R_{tn}, depth to the $CaCO_3$ layer followed by the SOC, were the most important factors. Depressions have deeper $CaCO_3$ layers than knolls, and the shallow $CaCO_3$ layer on knolls limited water infiltration during rainfall or snowmelt, resulting in less water recharge on knolls than in depressions. The depth to $CaCO_3$ layer and SOC were negatively correlated with elevation ($R = -0.54$, $P < 0.01$). Therefore, the influence of depth to $CaCO_3$ layer and SOC partially reflected the role of topography in driving snowmelt runoff along slopes in the spring, which contributes to increasing water recharge in depressions. Locations with greater SOC usually corresponded to vegetation with a larger leaf area index ($R = 0.23$, $P < 0.05$), which would also result in higher evapotranspiration and more water loss during discharge periods. As Table 1 shows, both depth to the $CaCO_3$ layer and SOC controlled time-stable patterns of SWC. This was because deeper $CaCO_3$ layers and higher SOC were observed in depressions where soils were usually wetter in most of the year because of the snowmelt runoff in the spring and rainfall runoff in the summer and autumn (van der Kamp et al., 2003). Therefore, the roles of soil and topography were two-fold: On one hand, they were highly correlated with the time-stable patterns and thus time stability of SWC (Gómez-Plaza et al., 2000; Mohanty and Skaggs, 2001; Grant et al., 2004); On the other hand, they, interplaying with temporal forcing, triggered local-specific soil water change and destroyed time stability of SWC. Their roles in protecting time stability persisted, but their roles in destroying time stability varied with time. Greater $\sigma^2_{\hat{n}}(R_{tn})$ implies greater contribution of these factors in soil water dynamics, resulting in less time stability of SWC.

The control of R_{tn} may be scale-specific, which can consequently affect the performance of the TA model. At a basin scale (31 500 km^2), Mittelbach and Seneviratne (2012) attributed the "static" factors such as soil texture and topography to time-stable spatial patterns, and meteorological conditions to temporal anomaly

HESSD
12, 6467–6503, 2015

(lumped $A_{t\hat{n}}$ and R_{tn}). At small scales, "static" factors such as depth to the $CaCO_3$ layer and SOC may affect not only the time-stable patterns but also the R_{tn}. The persistent influence of "static" factors on R_{tn} resulted in significant underlying spatial patterns in the R_{tn}. Thus, the TA model performed really well at the small scales, as demonstrated above. At large scales such as basin scale or greater, time-stable patterns may be controlled by, in addition to soil and topography, the climate gradient (Sherratt and Wheater, 1984); at those scales, R_{tn} is more likely to be controlled by the meteorological anomaly (i.e., spatially random variation) (Walsh and Mostek, 1980), and the effects of soil and topography may be reduced. Consequently, spatial patterns in the R_{tn} may be weakened and the TA model may have no advantages over the SA model at those large scales.

The different performance between the TA model and the SA model at the small watershed scales may be associated with the way EOF decomposition is performed. In the SA model, EOF decomposition is performed on lumped time-stable patterns $M_{\hat{t}n}$ and space-variant temporal anomaly R_{tn} (Perry and Niemann, 2007). In the TA model, however, EOF decomposition was made only on R_{tn}. In theory, the two models will be identical if $M_{\hat{t}n}$ and underlying spatial patterns (EOF1) of R_{tn} are perfectly correlated. In the TA model, $M_{\hat{t}n}$ and the underlying spatial patterns (EOF1) in R_{tn} were controlled by the same spatial forcing (e.g., depth to $CaCO_3$ layer and SOC) (Table 1), and they were correlated with an R^2 of 0.83 for the near surface and 0.42 for the root zone. Although the relationships between $M_{\hat{t}n}$ and R_{tn} were strong, they were not strictly linear, suggesting that $M_{\hat{t}n}$ and R_{tn} were affected differently by these factors. Because of a nonlinear relationship between them, lumping $M_{\hat{t}n}$ and R_{tn} together, as in the SA model, would weaken the model performance as compared to the TA model. From this aspect, the greater deviation from a linear relationship between $M_{\hat{t}n}$ and EOF1 of R_{tn}, lead to a greater outperformance of the TA model over the SA model.

The degree of outperformance of the TA model over the SA model also depends on the relative R_{tn} variance contribution to the total variance. Theoretically, the two models are also identical if variance of R_{tn} is zero or there are no interactions between

HESSD
12, 6467–6503, 2015

the spatial and temporal components (Fig. 1). Conversely, the greater variance of R_{tn}, the stronger the outperformance of the TA model. Therefore, the outperformance of the TA model over the SA model depends on counterbalance between the variance of R_{tn} and the linear correlation between $M_{\hat{t}n}$ and EOF1 of R_{tn}. For example, the variance of EOF1 in the R_{tn} for the near surface (i.e., 264 $\%^2$) was much greater than that for the root zone (i.e., 43 $\%^2$). However, $M_{\hat{t}n}$ and underlying spatial patterns (EOF1) in the R_{tn} in the root zone deviated more from a linear relationship. As a result, the outperformance of the TA model was comparable between the near surface and root zone (Fig. 9).

As demonstrated above, the R_{tn} destroys the time-stable patterns, and a greater value of $\sigma^2_{\hat{n}}(R_{tn})$ indicates less time-stable patterns. When SWC is close to average levels, R_{tn} is also close to zero, resulting in negligible variance contribution from R_{tn} to the total variance. In this case, the soil water patterns are stable, the SA model performs well, and there will be little differences between these two models. As is well known, the spatial patterns in soil water contents are inherently time unstable. For example, when evapotranspiration becomes the dominant process at the small watershed scale, more water will be lost in depressions due to the denser vegetation than on knolls (Millar, 1971; Biswas et al., 2012), effectively diminishing the spatial patterns and increasing temporal instability. In this case, the TA model may outperform the SA model. Therefore, the degree of outperformance of the TA model over the SA model depends on the amount of variances in the R_{tn} in addition to the degree of nonlinearity between the time-stable pattern $M_{\hat{t}n}$ and underlying spatial patterns in the R_{tn}. In the real world, the relations between the $M_{\hat{t}n}$ and underlying spatial patterns in the R_{tn} may rarely be perfectly linear. Therefore, when underlying spatial patterns exist in the R_{tn} and the R_{tn} has substantial variances, the TA model is preferable to the SA model for the estimation of spatially distributed SWC. Because the TA model was not worse than the SA model for the whole range of SWC, the TA model is suggested for the estimation of spatially distributed SWC at different soil water conditions.

HESSD
12, 6467–6503, 2015

Previous studies on SWC decomposition mainly focus on near surface layers (Jawson and Niemann, 2007; Perry and Niemann, 2007, 2008; Joshi and Mohanty, 2010; Korres et al., 2010; Busch et al., 2012). This study decomposed spatiotemporal SWC using the TA model for both the near surface and the root zone. The results showed that the estimation of spatially distributed SWC was improved by the TA method that considers R_{tn}. Because of the stronger time stability of SWC in deeper soil layers (Biswas and Si, 2011), SWC evaluation in thicker soil layers was more accurate than in shallow soil layers. This is particularly important because SWC data for deeper soil layers in a watershed is more difficult to collect than that of surface soil.

5 Conclusions

A statistical model (TA model) was used to decompose spatiotemporal SWC from a small watershed scale in the Canadian prairies, into time-stable patterns $M_{\hat{tn}}$, space-invariant temporal anomaly $A_{t\hat{n}}$, and space-variant temporal anomaly R_{tn}. The R_{tn} was further decomposed by an EOF analysis to reveal the underlying spatial patterns in the R_{tn}. The TA model was combined with time stability analysis to estimate spatially distributed SWC and was compared with the SA model, where the SWC was decomposed into spatial mean SWC and spatial anomaly Z_{tn}.

The contributions of spatial variance of the R_{tn} to the total variances of SWC were on average 118 and 19 % in the near surface and the root zone, respectively. There were significant persistent spatial patterns (EOFs) of R_{tn} over time, and the first pattern (EOF1) explained 61 and 44 % of the total variance in the R_{tn} for the near surface and root zone, respectively. Depth to the $CaCO_3$ layer and organic carbon content explained 81.6 % (0–0.2 m) and 81.0 % (0–1.0 m) of the variability in the EOF1 of R_{tn}. Compared to the SA model, estimation of spatially distributed SWC was improved with the TA model. This was because the TA model considered a fair amount of spatial variance in space-variant temporal anomaly, which was ignored in the SA model. Furthermore, the improved performance was observed mainly when soil water was

HESSD
12, 6467–6503, 2015

drier or wetter than the average level, especially in drier conditions due to the high $\sigma^2_{\hat{n}}(R_{tn})$ value. This study showed that outperformance of TA model over SA model is possible when $\sigma^2_{\hat{n}}(R_{tn})$ contributes substantial variance to the total variances of SWC, and significant spatial patterns (or EOFs) exist in the R_{tn}. Further application of the TA model for estimation of spatially distributed SWC at different scales and hydrological backgrounds is recommended. This study also implies a potential in using the TA model to construct a detailed spatially distributed SWC at watershed scales from remote sensed SWC. The codes for decomposing SWC with the SA and TA models and related EOF analysis were written in Matlab and are freely available from the authors upon request.

Acknowledgements. The project was funded by the Natural Sciences and Engineering Research Council (NSERC) of Canada. We thank Asim Biswas, Henry Wai Chau, Trent Pernitsky, and Eric Neil for their help in data collection.

References

Biswas, A. and Si, B. C.: Scales and locations of time stability of soil water storage in a hummocky landscape, J. Hydrol., 408, 100–112, doi:10.1016/j.jhydrol.2011.07.027, 2011.

Biswas, A., Chau, H. W., Bedard-Haughn, A., and Si, B. C.: Factors controlling soil water storage in the Hummocky landscape of the Prairie Pothole region of North America, Can. J. Soil Sci., 92, 649–663, doi:10.4141/CJSS2011-045, 2012.

Blöschl, G., Komma, J., and Hasenauer, S.: Hydrological downscaling of soil moisture, Final report to the H-SAF (Hydrology Satellite Application Facility) via the Austrian Central Institute for Meteorology and Geodynamics (ZAMG), Vienna University of Technology, Vienna, Austria, 2009.

Brocca, L., Melone, F., Moramarco, T., and Morbidelli, R.: Soil moisture temporal stability over experimental areas in Central Italy, Geoderma, 148, 364–374, doi:10.1016/j.geoderma.2008.11.004, 2009.

HESSD

12, 6467–6503, 2015

Brocca, L., Zucco, G., Mittelbach, H., Moramarco, T., and Seneviratne, S. I.: Absolute versus temporal anomaly and percent of saturation soil moisture spatial variability for six networks worldwide, Water Resour. Res., 50, 5560–5576, doi:10.1002/2014WR015684, 2014.

Burnham, K. P. and Anderson, D. R.: Model selection and multimodel inference: A practical information-theoretic approach, 2nd Edn., Springer-Verlag, New York, 2002.

Busch, F. A., Niemann, J. D., and Coleman, M.: Evaluation of an empirical orthogonal function-based method to downscale soil moisture patterns based on topographical attributes, Hydrol. Process., 26, 2696–2709, doi:10.1002/hyp.8363, 2012.

Champagne, C., Berg, A. A., McNairn, H., Drewitt, G., and Huffman, T.: Evaluation of soil moisture extremes for agricultural productivity in the Canadian prairies, Agr. Forest Meteorol., 165, 1–11, doi:10.1016/j.agrformet.2012.06.003, 2012.

Famiglietti, J. S., Rudnicki, J. W., and Rodell, M.: Variability in surface moisture content along a hillslope transect: Rattlesnake Hill, Texas, J. Hydrol., 210, 259–281, doi:10.1016/S0022-1694(98)00187-5, 1998.

Gómez-Plaza, A., Alvarez-Rogel, J., Albaladejo, J., and Castillo, V. M.: Spatial patterns and temporal stability of soil moisture across a range of scales in a semi-arid environment, Hydrol. Process., 14, 1261–1277, doi:10.1002/(SICI)1099-1085(200005)14:7<1261::AID-HYP40>3.0.CO;2-D, 2000.

Gómez-Plaza, A., Martínez-Mena, M., Albaladejo, J., and Castillo, V. M.: Factors regulating spatial distribution of soil water content in small semiarid catchments, J. Hydrol., 253, 211–226, doi:10.1016/S0022-1694(01)00483-8, 2001.

Grant, L., Seyfried, M., and McNamara, J.: Spatial variation and temporal stability of soil water in a snow-dominated, mountain catchment, Hydrol. Process., 18, 3493–3511, doi:10.1002/hyp.5789, 2004.

Grayson, R. B. and Western, A. W.: Towards areal estimation of soil water content from point measurements: Time and space stability of mean response, J. Hydrol., 207, 68–82, doi:10.1016/S0022-1694(98)00096-1, 1998.

Hu, W., Shao, M. A., and Reichardt, K.: Using a new criterion to identify sites for mean soil water storage evaluation, Soil Sci. Soc. Am. J., 74, 762–773, doi:10.2136/sssaj2009.0235, 2010.

Hu, W., Shao, M. A., Han, F. P., and Reichardt, K.: Spatio-temporal variability behavior of land surface soil water content in shrub- and grass-land, Geoderma, 162, 260–272, doi:10.1016/j.geoderma.2011.02.008, 2011.

HESSD
12, 6467–6503, 2015

Hu, W., Tallon, L. K., and Si, B. C.: Evaluation of time stability indices for soil water storage upscaling, J. Hydrol., 475, 229–241, doi:10.1016/j.jhydrol.2012.09.050, 2012.
Jawson, S. D. and Niemann, J. D.: Spatial patterns from EOF analysis of soil moisture at a large scale and their dependence on soil, land-use, and topographic properties, Adv. Water Resour., 30, 366–381, doi:10.1016/j.advwatres.2006.05.006, 2007.
Jia, Y. H. and Shao, M. A.: Temporal stability of soil water storage under four types of revegetation on the northern Loess Plateau of China, Agr. Water Manage., 117, 33–42, doi:10.1016/j.agwat.2012.10.013, 2013.
Johnson, R. A. and Wichern, D. W.: Applied multivariate statistical analysis, Prentice Hall, Upper Saddle River, New Jersey, 2002.
Joshi, C. and Mohanty, B. P.: Physical controls of near-surface soil moisture across varying spatial scales in an agricultural landscape during SMEX02, Water Resour. Res., 46, W12503, doi:10.1029/2010WR009152, 2010.
Korres, W., Koyama, C. N., Fiener, P., and Schneider, K.: Analysis of surface soil moisture patterns in agricultural landscapes using Empirical Orthogonal Functions, Hydrol. Earth Syst. Sci., 14, 751–764, doi:10.5194/hess-14-751-2010, 2010.
Martínez-Fernández, J. and Ceballos, A.: Temporal stability of soil moisture in a large-field experiment in Spain, Soil Sci. Soc. Am. J., 67, 1647–1656, 2003.
Millar, J. B.: Shoreline-area ratios as a factor in rate of water loss from small sloughs, J. Hydrol., 14, 259–284, doi:10.1016/0022-1694(71)90038-2, 1971.
Mittelbach, H. and Seneviratne, S. I.: A new perspective on the spatio-temporal variability of soil moisture: temporal dynamics versus time-invariant contributions, Hydrol. Earth Syst. Sci., 16, 2169–2179, doi:10.5194/hess-16-2169-2012, 2012.
Mohanty, B. P. and Skaggs, T. H.: Spatio-temporal evolution and time–stable characteristics of soil moisture within remote sensing footprints with varying soil slope and vegetation, Adv. Water Resour., 24, 1051–1067, doi:10.1016/S0309-1708(01)00034-3, 2001.
Peel, M. C., Finlayson, B. L., and McMahon, T. A.: Updated world map of the Köppen–Geiger climate classification, Hydrol. Earth Syst. Sci., 11, 1633–1644, doi:10.5194/hess-11-1633-2007, 2007.
Perry, M. A. and Niemann J. D.: Analysis and estimation of soil moisture at the catchment scale using EOFs, J. Hydrol., 334, 388–404, doi:10.1016/j.jhydrol.2006.10.014, 2007.
Perry, M. A. and Niemann, J. D.: Generation of soil moisture patterns at the catchment scale by EOF interpolation, Hydrol. Earth Syst. Sci., 12, 39–53, doi:10.5194/hess-12-39-2008, 2008.

HESSD
12, 6467–6503, 2015

Robinson, D. A., Campbell, C. S., Hopmans, J. W., Hornbuckle, B. K., Jones, S. B., Knight, R., Ogden, F., Selker, J., and Wendroth, O.: Soil moisture measurement for ecological and hydrological watershed-scale observatories: A review, Vadose Zone J., 7, 358–389, doi:10.2136/vzj2007.0143, 2008.

Rötzer, K., Montzka, C., and Vereecken, H.: Spatio-temporal variability of global soil moisture products, J. Hydrol., 522, 187–202, doi:10.1016/j.jhydrol.2014.12.038, 2015.

She, D. L., Liu, D. D., Peng, S. Z., and Shao, M. A.: Multiscale influences of soil properties on soil water content distribution in a watershed on the Chinese Loess Plateau, Soil Sci., 178, 530–539, doi:10.1016/j.jhydrol.2014.08.034, 2013a.

She, D. L., Xia, Y. Q., Shao, M. A., Peng, S. Z., and Yu, S. E.: Transpiration and canopy conductance of Caragana Korshinskii trees in response to soil moisture in sand land of China, Agroforest. Syst., 87, 667–678, doi:10.1007/s10457-012-9587-4, 2013b.

Sherratt, D. J. and Wheater, H. S.: The use of surface-resistance soil-moisture relationships in soil-water budget models, Agr. Forest Meteorol., 31, 143–157, doi:10.1016/0168-1923(84)90016-9, 1984.

Soil Survey Staff: Soil Taxonomy, 11th Edn., USDA National Resources Conservation Services, Washington DC, 2010.

Starr, G. C.: Assessing temporal stability and spatial variability of soil water patterns with implications for precision water management, Agr. Water Manage., 72, 223–243, doi:10.1016/j.agwat.2004.09.020, 2005.

Vachaud, G., De Silans, A. P., Balabanis, P., and Vauclin, M.: Temporal stability of spatially measured soil water probability density function, Soil Sci. Soc. Am. J., 49, 822–828, 1985.

van der Kamp, G., Hayashi, M., and Gallen, D.: Comparing the hydrology of grassed and cultivated catchments in the semi-arid Canadian prairies, Hydrol. Process., 17, 559–575, doi:10.1002/hyp.1157, 2003.

Vanderlinden, K., Vereecken, H., Hardelauf, H., Herbst, M., Martinez, G., Cosh, M. H., and Pachepsky, Y. A.: Temporal stability of soil water contents: A review of data and analyses, Vadose Zone J., 11, 4, doi:10.2136/vzj2011.0178, 2012.

Vereecken, H., Kamai, T., Harter, T., Kasteel, R., Hopmans, J., and Vanderborght, J.: Explaining soil moisture variability as a function of mean soil moisture: A stochastic unsaturated flow perspective, Geophys. Res. Lett., 34, L22402, doi:10.1029/2007GL031813, 2007.

HESSD
12, 6467–6503, 2015

Venkatesh, B., Nandagiri, L., Purandara, B. K., and Reddy, V. B.: Modelling soil moisture under different land covers in a sub-humid environment of Western Ghats, India, J. Earth Syst. Sci., 120, 387–398, 2011.

Walsh, J. E. and Mostek, A.: A quantitative-analysis of meteorological anomaly patterns over the United-States, 1900–1977, Mon. Weather Rev., 108, 615–630, doi:10.1175/1520-0493(1980)108< 0615:AQAOMA>2.0.CO;2, 1980.

Wang, Y. Q., Shao, M. A., Liu, Z. P., and Warrington, D. N.: Regional spatial pattern of deep soil water content and its influencing factors, Hydrolog. Sci. J., 57, 265–281, doi:10.1080/02626667.2011.644243, 2012.

Ward, P. R., Flower, K. C., Cordingley, N., Weeks, C., and Micin, S. F.: Soil water balance with cover crops and conservation agriculture in a Mediterranean climate, Field Crop. Res., 132, 33–39, doi:10.1016/j.fcr.2011.10.017, 2012.

Zhao, Y., Peth, S., Wang, X. Y., Lin, H., and Horn, R.: Controls of surface soil moisture spatial patterns and their temporal stability in a semi-arid steppe, Hydrol. Process., 24, 2507–2519, doi:10.1002/hyp.7665, 2010.

HESSD

12, 6467–6503, 2015

Table 1. Pearson correlation coefficients between time-stable pattern $M_{\hat{t}n}$, EOF1 of space-variant temporal anomaly R_{tn} and various properties.

	0–0.2 m		0–1.0 m	
	$M_{\hat{t}n}$	EOF1	$M_{\hat{t}n}$	EOF1
Sand content	−0.52**	−0.36**	−0.66**	−0.26**
Silt content	0.29**	0.14	0.40**	0.06
Clay content	0.43**	0.38**	0.51**	0.33**
Organic carbon	0.78**	0.83**	0.73**	0.76**
Wetness index	0.64**	0.59**	0.68**	0.56**
Depth to $CaCO_3$ layer	0.77**	0.84**	0.65**	0.88**
A horizon depth	0.51**	0.62**	0.44**	0.65**
C horizon depth	0.66**	0.69**	0.58**	0.76**
Bulk density	−0.58**	−0.67**	−0.46**	−0.62**
Elevation	−0.24**	−0.28**	−0.24**	−0.32**
Specific contributing area	0.20*	0.24**	0.24**	0.23**
Convergence index	−0.58**	−0.56**	−0.55**	−0.58**
Curvature	−0.10	−0.08	−0.19*	−0.16
Cos(aspect)	0.05	0.04	0.08	0.05
Gradient	−0.12	−0.09	−0.21*	−0.02
Slope	−0.51**	−0.48**	−0.56**	−0.44**
Upslope length	0.19*	0.21*	0.21*	0.25**
Solar radiation	−0.07	0.03	−0.11	0.08
Flow connectivity	0.45**	0.43**	0.49**	0.49**
Leaf area index	−0.07	0.06	−0.10	−0.14
Variance explained[1]	74.5 %	81.6 %	75.6 %	81.0 %

[1] Percent of variance explained by the controlling factors obtained by the multiple stepwise regressions.
* significant at $P < 0.05$; ** significant at $P < 0.01$.

HESSD
12, 6467–6503, 2015

Table A1. Notations.

$M_{\hat{t}\hat{n}}$	spatial mean of $M_{\hat{t}n}$
R_{tn}	space-variant temporal anomaly of SWC at location n and time t
$A_{t\hat{n}}$	space-invariant temporal anomaly of SWC at time t
Z_{tn}	spatial anomaly of SWC at location n and time t
$S_{t\hat{n}}$	spatial mean SWC at time t
$\sigma^2_{\hat{n}}$	spatial variance
A_{tn}	temporal anomaly of SWC at location n and time t
$\delta_{\hat{t}n}$	temporal mean relative difference of SWC at location n
cov	spatial covariance
S_{tn}	SWC at location n and time t
$M_{\hat{t}n}$	time-stable pattern of SWC
ECs	temporally-varying coefficients of R_{tn} (or Z_{tn})
EOFs	time-invariant spatial structures of R_{tn} (or Z_{tn})
NSCE	Nash–Sutcliffe coefficient of efficiency
R	Pearson correlation coefficient
SWC	soil water content

HESSD
12, 6467–6503, 2015

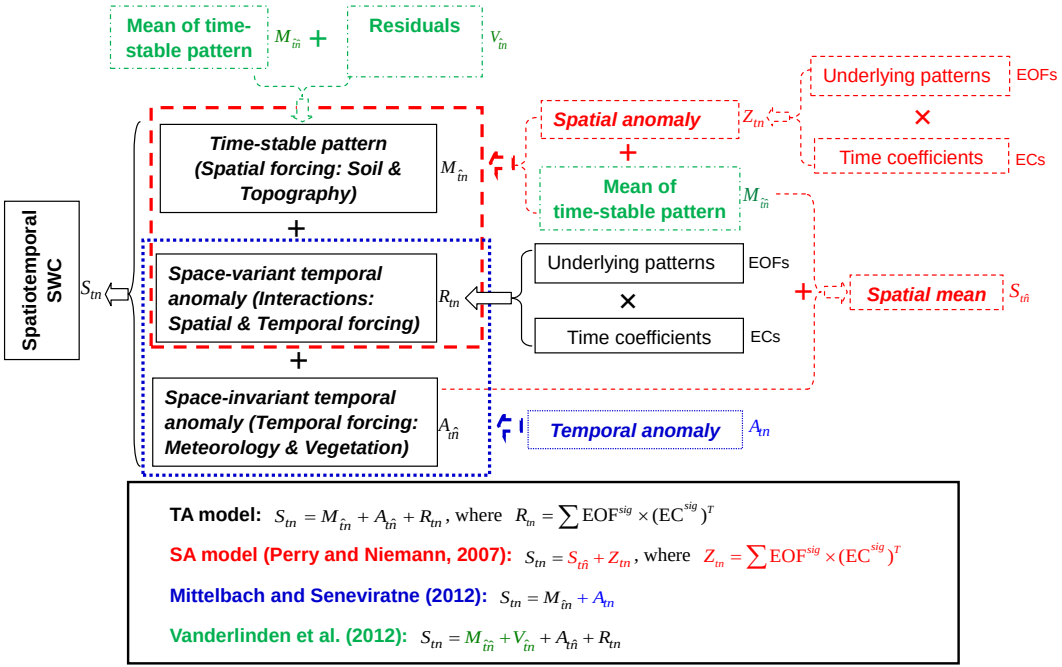

Figure 1. Decomposition of spatiotemporal soil water content (SWC) in different models.

HESSD
12, 6467–6503, 2015

Estimating spatially distributed soil water content at small watershed scales

W. Hu and B. C. Si

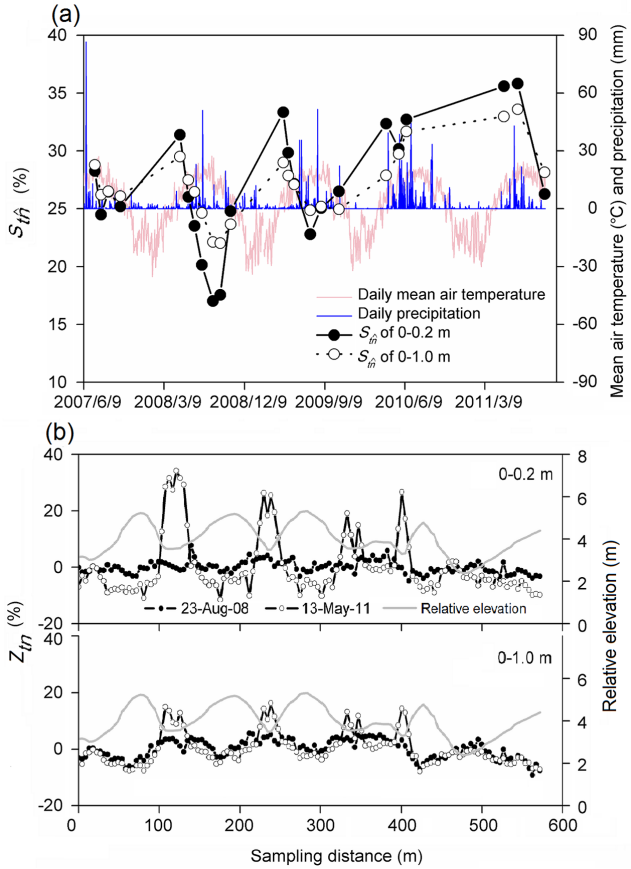

Figure 2. Components of soil water content in the SA model: **(a)** spatial mean soil water content $S_{t\hat{n}}$ and **(b)** spatial anomaly Z_{tn} on a dry day (23 August 2008) and a wet day (13 May 2011) for 0–0.2 and 0–1.0 m. Also shown is the relative elevation.

HESSD
12, 6467–6503, 2015

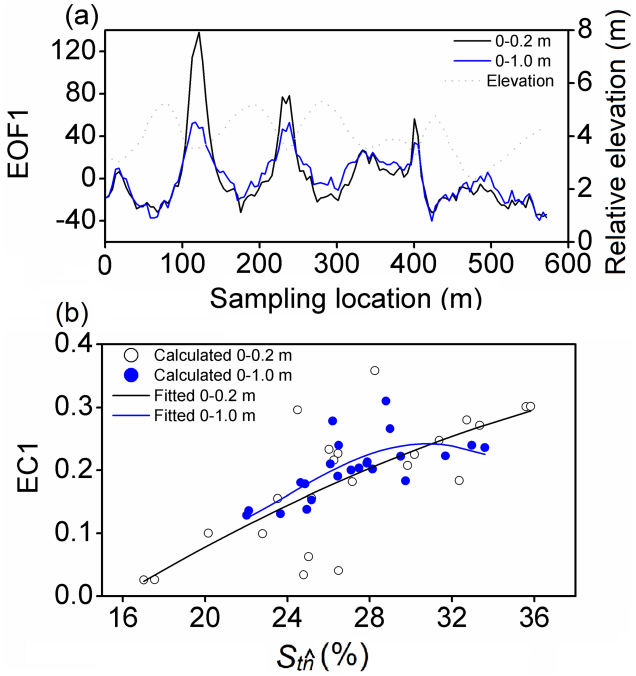

Figure 3. (a) The EOF1 of the spatial anomaly Z_{tn} and **(b)** relationships of associated EC1 versus spatial mean soil water content Z_{tn} fitted by the cosine function (Eq. 4).

HESSD
12, 6467–6503, 2015

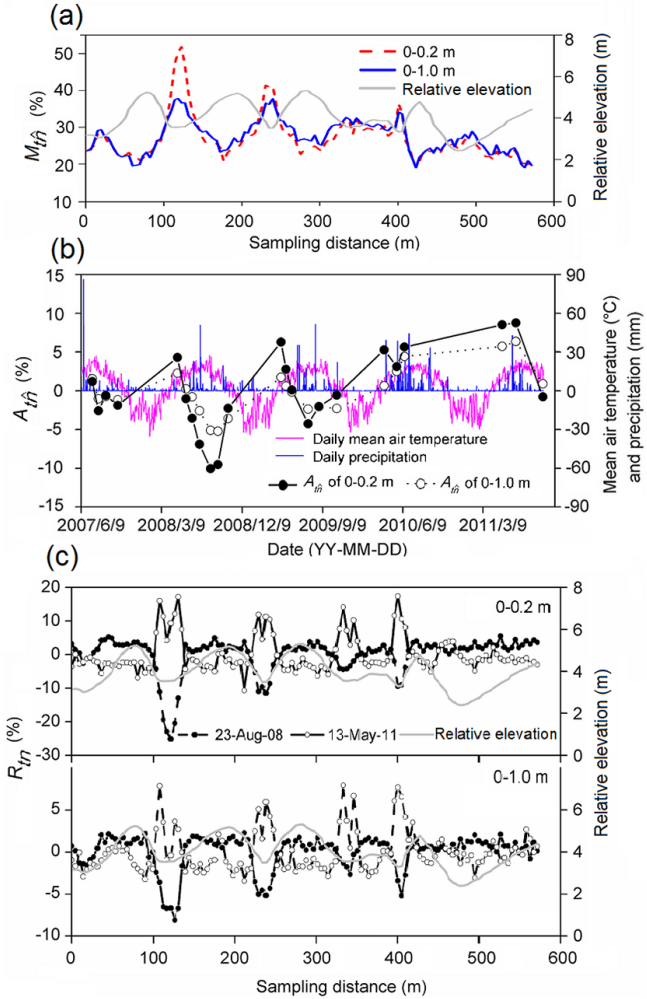

HESSD
12, 6467–6503, 2015

Estimating spatially distributed soil water content at small watershed scales

W. Hu and B. C. Si

Figure 4. Components of soil water content of the TA model: **(a)** time-stable pattern $M_{\hat{t}n}$, **(b)** space-invariant temporal anomaly $A_{t\hat{n}}$, and **(c)** space-variant temporal anomaly R_{tn} on a dry day (23 August 2008) and a wet day (13 May 2011) for 0–0.2 and 0–1.0 m. Also shown are relative elevation, daily mean air temperature, and daily precipitation.

HESSD
12, 6467–6503, 2015

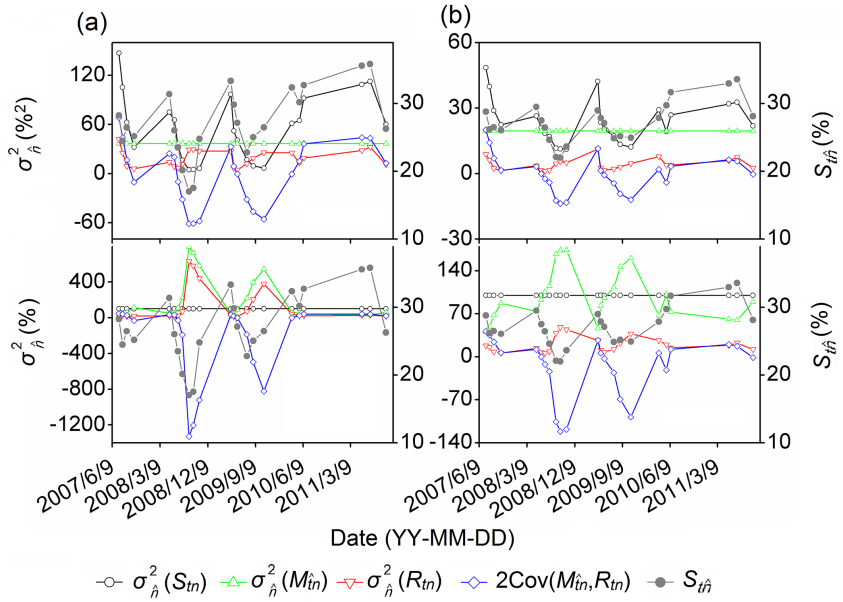

Figure 5. Spatial variances of different components in Eq. (8) expressed in $\%^2$ (upper panel) and as percentage (lower panel) for **(a)** 0–0.2 m and **(b)** 0–1.0 m. Spatial mean soil water content $S_{t\hat{n}}$ on each measurement day is also shown.

HESSD
12, 6467–6503, 2015

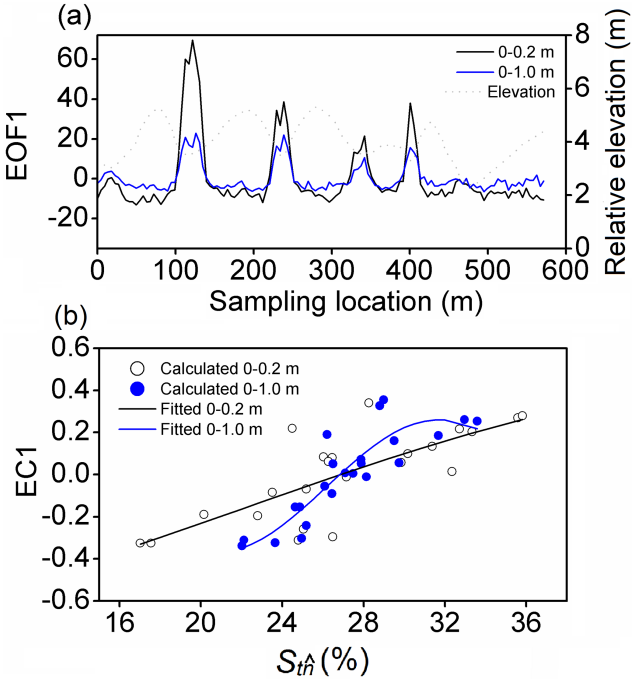

Figure 6. (a) The EOF1 of the space-variant temporal anomaly R_{tn} and **(b)** relationships of associated EC1 versus spatial mean soil water content $S_{t\hat{n}}$ fitted by the cosine function (Eq. 4).

HESSD
12, 6467–6503, 2015

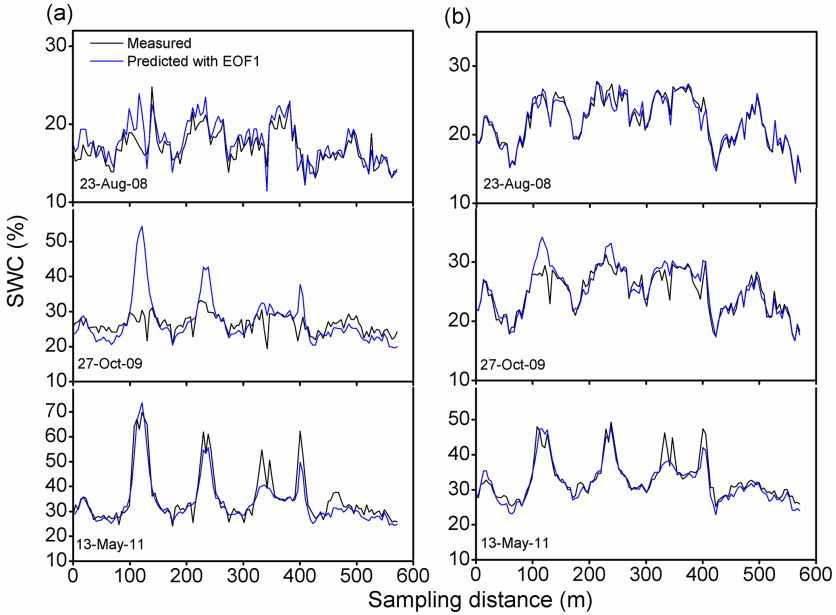

Figure 7. Estimated soil water content (SWC) versus measured SWC for three dates at different soil water conditions (23 August 2008, 27 October 2009, and 13 May 2011 are associated with relatively dry, medium, and wet days, respectively) using the TA model for **(a)** 0–0.2 m and **(b)** 0–1.0 m.

HESSD
12, 6467–6503, 2015

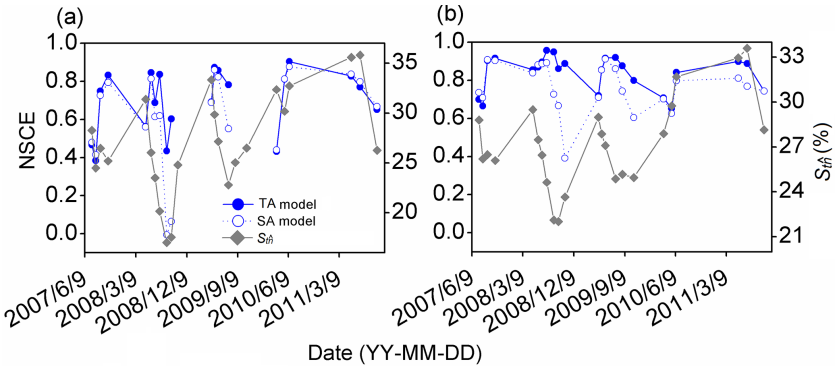

Figure 8. The Nash–Sutcliffe coefficient of efficiency (NSCE) of soil water content estimation using the TA and SA models at **(a)** 0–0.2 m and **(b)** 0–1.0 m. At 0–0.2 m, negative Nash–Sutcliffe coefficient of efficiency values for three dates (22 October 2008, 27 August 2009, and 27 October 2009) are not shown. Spatial mean soil water content $S_{t\hat{n}}$ on each measurement day is also shown.

HESSD
12, 6467–6503, 2015

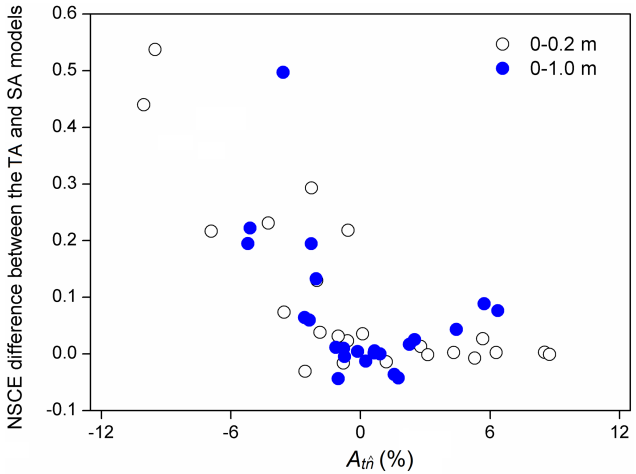

Figure 9. Difference between the Nash–Sutcliffe coefficient of efficiency (NSCE) of soil water content evaluation using the TA and the SA models as a function of space-invariant temporal anomaly $A_{t\hat{n}}$ at **(a)** 0–0.2 m and **(b)** 0–1.0 m.

HESSD
12, 6467–6503, 2015